Efficient, non-iterative estimator for imaging contrast agents with spectral x-ray detectors

Robert E. Alvarez

***Abstract*—An estimator to image contrast agents and body materials with x-ray spectral measurements is described. The estimator is usable with the three or more basis functions that are required with high atomic number materials. The estimator variance is equal to the Cramèr-Rao lower bound (CRLB) and it is unbiased. Its parameters are computed from measurements of a calibration phantom with the clinical x-ray system and it is non-iterative. The estimator is compared with an iterative maximum likelihood estimator. Methods: The estimator first computes a linearized maximum likelihood estimate of the line integrals of the basis set. Corrections for bias errors in the initial estimates are computed by interpolation with calibration phantom data. The final estimate is the initial estimate plus the correction. The estimator parameters are computed from measurements of a calibration phantom with the clinical x-ray system. The performance of the estimator is measured using a Monte Carlo simulation. Random photon counting with pulse height analysis data are generated. The mean squared errors of the estimates are compared to the CRLB. The random data are also processed with an iterative maximum likelihood estimator. Previous implementations of iterative estimators required advanced physics instruments not usually available in clinical institutions. Results: The estimator mean squared error (MSE) is essentially equal to the CRLB. The estimator outputs are close to those of the iterative estimator. The computation time is approximately 180 times shorter than the iterative implementation. Conclusion: The estimator is efficient and has advantages over alternate approaches such as iterative estimators.**

Key Words: spectral CT, dual energy, energy selective, Cramèr-Rao lower bound, Monte Carlo, maximum likelihood estimator, iterative estimator

I. INTRODUCTION

The state of the art of photon counting detectors is advancing rapidly and their use in clinical systems may be possible in the near future[1], [2]. These detectors have the capability to measure the energy of the individual photons with pulse height analysis (PHA). Since each PHA energy bin can be considered to provide a separate spectral measurement, they have the potential to provide many more spectra than were previously available and methods to process this information are required.

This paper describes an estimator that uses these multiple x-ray spectrum measurements to extract energy dependent information optimally. The estimator is efficient over a large range of object thicknesses with variance essentially equal to the Cramèr-Rao lower bound (CRLB) and with bias much smaller than the noise standard deviation. The estimator is non-iterative and the parameters required to implement it can be computed from measurements of a calibration phantom with the clinical x-ray system. The rationale for the estimator is described and its use is justified by its empirical performance measured with a Monte Carlo simulation.

The estimator implements a key step in the Alvarez-Macovski method[3]. With this method, the x-ray attenuation coefficient is approximated as a linear combination of basis functions of energy multiplied by coefficients that are independent of energy. The estimator uses measurements of the number of photons transmitted through the object with different spectra to compute the line integrals of the basis set coefficients. The vector of these line integrals will be referred to as the A-vector here.

The number of basis functions, the dimensionality, determines the available information and the minimum number of spectra required to extract it[4]. A two function basis set is sufficient to approximate the attenuation coefficients of biological materials[3]. However, a three or higher dimension basis set is needed if an externally administered high atomic number contrast agent is used. In this case, measurements with three or more effective spectra are required.

A previous paper[5] described a two dimension estimator[6], [7]. Because of the two dimension limitation, this implementation could not be used with contrast agents. In this paper, a new estimator is described that is usable with three or more basis functions as well as two functions.

The rationale for the estimator is based on the near linearity of the logarithm of the number of photons transmitted through the object as a function of the A-vector. Assuming a linear system and a multivariate normal distribution, the linear maximum likelihood estimator (linear MLE) is the minimum variance unbiased estimator[8]. Because the nonlinearity is small, the variance of the linear estimates is close to the CRLB of the actual, nonlinear system. The nonlinearity, however, leads to bias of the linear estimates that needs to be minimized for quantitative applications such as computed tomography (CT). This is done by correcting the initial estimates based on known calibration data. The final estimate is the initial estimate plus the correction. Since the correction values are computed from a table of A-vector values, the estimator is called the A-table estimator.

A method to compute the parameters of the estimator from measurements of a calibration phantom with the clinical x-ray system is described. The design of the calibrator and ways to compute the estimator parameters

from the data are shown.

The performance of the estimator is tested with a Monte Carlo simulation using realistic models of an x-ray tube spectrum and x-ray attenuation coefficients. The random Monte Carlo data are generated using the full nonlinear transmitted spectrum model. The estimator operates on the random data and the covariance of the A-vector estimates is compared to the fundamental Cramèr-Rao lower bound (CRLB), which is the minimum covariance for any unbiased estimator[9]. To do this comparison, the mean squared error (MSE) of the A-vector estimates is compared with the CRLB. Using the well-known fact that the MSE is the variance plus the square of the bias[10] and since both of these quantities are positive, if the MSE is equal to the CRLB, which is the minimum variance, then we can conclude that the bias is negligible and the estimator is efficient.

Prior estimators for higher dimensions[11], [12] utilized an iterative implementation of the maximum likelihood method. Even though maximum likelihood estimators have many desirable properties[13], this implementation required separate measurements of the x-ray tube source spectrum and the detector spectral response. In the experiments, the source spectrum was measured using a cooled germanium detector with energy resolution of a few hundred electron-volts. The PHA energy bin thresholds were measured using the DESY synchrotron radiation nuclear physics accelerator[14] to provide nearly monoenergetic tunable x-ray radiation. See their paper for a detailed description of the experimental technique.

Although these are extremely impressive results, this experimental method is not practical with the facilities commonly available at clinical institutions. Due to component aging, the sputtering of x-ray tube anode material on the x-ray tube window and other effects, spectral x-ray systems need to be calibrated periodically so an estimator whose parameters can be measured at clinical sites is required. Iterative estimators also have possible problems with stability and have long and unpredictable computation times. This is a problem for modern medical x-ray systems such as CT scanners that require real-time computations in fixed times.

To test the performance of the A-table estimator, it is compared with an iterative maximum likelihood estimator that assumes that the source spectrum and the PHA detector energy bins are known.

II. METHODS

The estimator and its operation are described in Fig. 1. In order to apply the concept to higher dimensions, we need interpolators for multidimensional non-regularly spaced data and a multidimensional calibrator with a method to compute the estimator parameters from its data. An iterative maximum likelihood estimator for comparison with the A-table estimator is also described in this section.

A. The A-space method in higher dimensions

This section summarizes the Alvarez-Macovski method and introduces notation. A two dimension basis set is sufficient to approximate the attenuation coefficients of body materials accurately but, with a high atomic number contrast agent, we need three or more functions[4]. In the three dimension case, the attenuation coefficient $\mu(\mathbf{r}, E)$ at each point $\mathbf{r}$ in the object at energy E is

$$\mu(\mathbf{r}, E) = a_1(\mathbf{r}) f_1(E) + a_2(\mathbf{r}) f_2(E) + a_3(\mathbf{r}) f_3(E) \qquad (1)$$

where $a_i(\mathbf{r})$ are the basis set coefficients and $f_i(E)$ are the basis functions, $i = 1 \ldots 3$. As implied by the notation, the basis set coefficients $a_i(\mathbf{r})$ are functions only of the position within the object and the basis functions $f_i(E)$ are functions only of the x-ray energy. The extension to higher A-vector dimensions is straight forward.

Neglecting scatter, if an effective measurement spectrum $S_k(E)$ is used, the expected value of the number of transmitted photons n_k is

$$\lambda_k = \langle n_k \rangle = \int S_k(E) e^{-\int \mu(\mathbf{r},E) d\mathbf{r}} dE, \ k = 1, \ldots, \ nspect \qquad (2)$$

where $nspect$ is the number of spectral measurements and $\langle\ \rangle$ denotes expected value. Using (1), the line integral can be expressed as

$$\int \mu(\mathbf{r}, E)\, d\mathbf{r} = A_1 f_1(E) + A_2 f_2(E) + A_3 f_3(E). \qquad (3)$$

where $A_i = \int a_i(\mathbf{r})\, d\mathbf{r}, \ i = 1 \ldots 3$. The A_i are the components of the A-vector $\mathbf{A}$ and the measurements can be summarized by a vector $\mathbf{N}$ whose components are the measurements n_k with the different spectra.

In an x-ray system, the measurements have noise and the Alvarez-Macovski method requires an estimator to compute the best estimate of the A-vector taking into account the probability distribution of the measurements.

B. The maximum likelihood estimator with x-ray spectral data

The maximum likelihood estimator[13] is widely used because it is asymptotically efficient in the limit of large photon counts. Since large counts are required for material selective imaging applications, the maximum likelihood approach is well suited for these applications.

Assuming that the PHA detector counts are independent and Poisson distributed, the likelihood function, which is the probability of a particular measurement $\mathbf{N}$ considered to be a function of $\mathbf{A}$, is

$$Pr\left[\mathbf{N}(\mathbf{A})\right] = \prod_{k=1}^{nspect} \frac{e^{-\lambda_k(\mathbf{A})} \lambda_k^{n_k}(\mathbf{A})}{n_k!} \qquad (4)$$

where the expected values $\lambda_k(\mathbf{A})$ are given by (2) and n_k is the measurement with spectrum k. The maximum

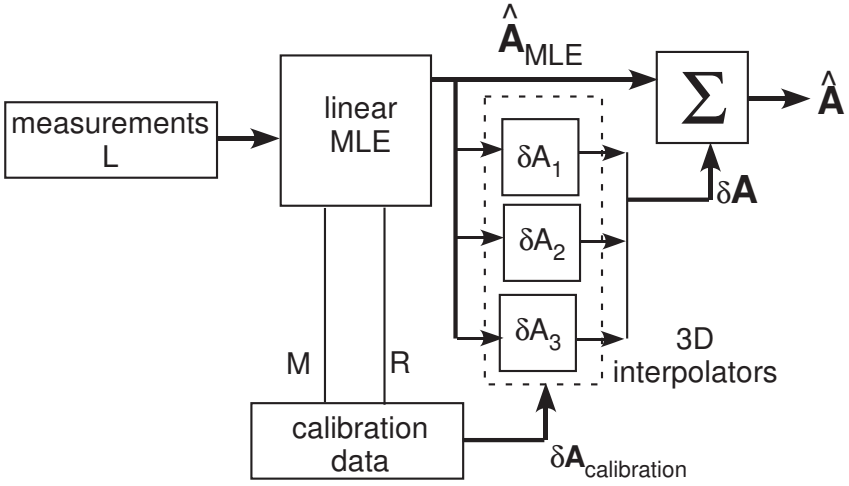

Fig. 1. A-table estimator block diagram. The estimator first computes an initial estimate $\hat{\mathbf{A}}_{MLE}$ with a linearized maximum likelihood estimator (linear MLE). Because the mapping from measurements to object attenuation is non-linear, these initial estimates will have errors. The error vectors are determined at a set of points in a three dimensional space from measurements on a calibration phantom and stored in the memory labeled "calibration data." During image acquisition, the $\hat{\mathbf{A}}_{MLE}$ is used to compute an error vector with components $\delta_{A_{1\ldots3}}$ by multidimensional interpolation. The final estimator output is the initial linear MLE plus the correction vector, $\hat{\mathbf{A}} = \hat{\mathbf{A}}_{MLE} + \delta\mathbf{A}$.

likelihood estimate $\hat{\mathbf{A}}_{MLE}$ is the value of $\mathbf{A}$ that maximizes (4). It is convenient and equivalent to maximize the logarithm of the likelihood

$$\mathcal{L}(\mathbf{A}) = \sum_{k=1}^{nspect} n_k \log(\lambda_k) - \lambda_k - \log(n_k!). \qquad (5)$$

We can attempt to find the maximum by setting the derivatives of $\mathcal{L}(\mathbf{A})$ equal to zero

$$\frac{\partial \mathcal{L}}{\partial A_i} = \sum_{k=1}^{nspect} \frac{\partial \lambda_k}{\partial A_i}\left(\frac{n_k}{\lambda_k} - 1\right) = 0,\ i = 1 \ldots ndim, \qquad (6)$$

where $ndim$ is the A-vector dimension.

Defining $z_k = (n_k/\lambda_k - 1)$, equations (6) are a set of $ndim$ linear homogeneous equations in $nspect$ unknowns, $z_k,\ k = 1, \ldots, nspect$

$$\begin{aligned} \tfrac{\partial \lambda_1}{\partial A_1} z_1 + \tfrac{\partial \lambda_2}{\partial A_1} z_2 + \ldots \tfrac{\partial \lambda_{nspect}}{\partial A_1} z_{nspect} &= 0 \\ \ddots \qquad\qquad &= 0 \\ \tfrac{\partial \lambda_1}{\partial A_{ndim}} z_1 + \tfrac{\partial \lambda_2}{\partial A_{ndim}} z_2 + \ldots \tfrac{\partial \lambda_{nspect}}{\partial A_{ndim}} z_{nspect} &= 0 \end{aligned} \qquad (7)$$

If the number of spectral measurements is equal to the A-vector dimension and the determinant of the coefficients matrix

$$J = \det \begin{bmatrix} \frac{\partial \lambda_1}{\partial A_1} & \cdots & \frac{\partial \lambda_{nspect}}{\partial A_1} \\ & \ddots & \\ \frac{\partial \lambda_1}{\partial A_{ndim}} & \cdots & \frac{\partial \lambda_{nspect}}{\partial A_{ndim}} \end{bmatrix} \neq 0$$

is not equal to zero, the unique solution is

$$z_k = \left(\frac{n_k}{\lambda_k} - 1\right) = 0,\ k = 1 \ldots nspect. \qquad (8)$$

Note that the determinant of the coefficients J is the Jacobian of the transformation $\mathbf{N}(\mathbf{A})$, which will be nonzero if the measurement spectra are distinct.

Eq. 8 is equivalent to $n_k = \lambda_k$ so for the equal number of measurements and dimensions case the maximum likelihood estimator simply inverts the deterministic or low noise transformation given by (2) with the measured data. Therefore, any estimator that accurately inverts the transformation is also the maximum likelihood estimator[3].

If there are more measurement spectra than the A-vector dimension, then equations (7) have more unknowns, $z_k,\ k = 1 \ldots nspect$, than the $ndim$ equations. This does not in general have a unique solution and inverting the deterministic transformation with the measured data is not necessarily the maximum likelihood estimator. In this case we need an alternative implementation such as the iterative estimator described in Sec. II-J or the A-table estimator.

C. CRLB for A-vector estimates

The CRLB is the minimum covariance for any estimator and is a cornerstone of estimator theory. In general, it is inverse of the Fisher information matrix $\mathbf{F}$ whose elements are[9]

$$F_{ij} = -\left\langle \frac{\partial^2 \mathcal{L}}{\partial A_i \partial A_j} \right\rangle \qquad (9)$$

where, it will be recalled, the symbol $\langle\ \rangle$ denotes the expected value. The first derivative of the log-likelihood $\mathcal{L}$ is given by the left side of (6). Differentiating again

$$\begin{aligned} \tfrac{\partial^2 \mathcal{L}}{\partial A_i \partial A_j} &= \textstyle\sum_{k=1}^{nspect} \tfrac{\partial^2 \lambda_k}{\partial A_i \partial A_j}\left[\tfrac{n_k - \lambda_k}{\lambda_k}\right] \cdots \\ &\quad -\tfrac{1}{\lambda_k}\tfrac{\partial \lambda_k}{\partial A_i}\left[1 + \tfrac{n_k - \lambda_k}{\lambda_k}\right]\tfrac{\partial \lambda_k}{\partial A_j}. \end{aligned} \qquad (10)$$

Since by the definition of λ_k, the expected value $\langle n_k - \lambda_k \rangle = \langle n_k \rangle - \lambda_k = 0$, the expected value of the first term in the summand of (10) is equal to zero and the

expected value of the second term is

$$\left\langle \frac{1}{\lambda_k}\frac{\partial\lambda_k}{\partial A_i}\left[1+\frac{n_k-\lambda_k}{\lambda_k}\right]\frac{\partial\lambda_k}{\partial A_j}\right\rangle = \frac{1}{\lambda_k}\frac{\partial\lambda_k}{\partial A_i}\frac{\partial\lambda_k}{\partial A_j} = \left[\frac{1}{\lambda_k}\frac{\partial\lambda_k}{\partial A_i}\right]\lambda_k\left[\frac{1}{\lambda_k}\frac{\partial\lambda_k}{\partial A_j}\right].$$

Therefore, the element of the Fisher matrix in (9) is

$$F_{ij} = -\left\langle \frac{\partial^2\mathcal{L}}{\partial A_i \partial A_j}\right\rangle = \sum_{k=1}^{nspect}\left[\frac{1}{\lambda_k}\frac{\partial\lambda_k}{\partial A_i}\right]\lambda_k\left[\frac{1}{\lambda_k}\frac{\partial\lambda_k}{\partial A_j}\right]. \quad (11)$$

The terms in the brackets of (11) can be computed without numerical differentiation by differentiating inside the integral of the equation for the expected values of the counts, (2),

$$\left[\frac{1}{\lambda_k}\frac{\partial\lambda_k}{\partial A_i}\right] = -\frac{\int S_k(E) f_i(E) e^{-\sum A_m f_m(E)} dE}{\int S_k(E) e^{-\sum A_m f_m(E)} dE}. \quad (12)$$

Defining the normalized spectrum transmitted through the object

$$\hat{S}_k(\mathbf{A}, E) = \frac{S_k(E) e^{-\sum A_m f_m(E)}}{\int S_k(E) e^{-\sum A_m f_m(E)} dE},$$

we can see that the terms in the brackets of (11) are the negatives of the elements of a matrix $\mathbf{M}(\mathbf{A})$ of the effective values of the basis functions in the normalized transmitted spectra,

$$M_{ki} = \int f_i(E)\hat{S}_k(\mathbf{A}, E) dE = \langle f_i \rangle_{S_k}.$$

The number of rows of $\mathbf{M}$ is the number of spectra and the number of columns is the A-vector dimension. As implied by the notation, in general $\mathbf{M}$ and the CRLB depend on the A-vector.

Since the PHA count data are assumed to be independent and Poisson distributed, the covariance is the diagonal matrix

$$\mathbf{C_N}(\mathbf{A}) = \begin{bmatrix} \lambda_1(\mathbf{A}) & & 0 \\ & \cdots & \\ 0 & & \lambda_{nspect}(\mathbf{A}) \end{bmatrix} \quad (13)$$

Using equations (12) and (13) with (11), the complete Fisher matrix is

$$\mathbf{F}(\mathbf{A}) = \mathbf{M^T C_N M}. \quad (14)$$

This can be shown in detail by carrying out the indicated matrix multiplications. Given the Fisher matrix, the CRLB can be computed as the numerical inverse.

D. The linear maximum likelihood estimator in higher dimensions

As shown in Fig. 1, the A-table estimator uses a linearized maximum likelihood estimator. Since the body transmission is exponential in $\mathbf{A}$, we can approximately linearize the measurements by taking logarithms. The results is the log measurement vector $\mathbf{L} = -\log(\mathbf{N}/\mathbf{N_0})$, where $\mathbf{N_0}$ is the expected value of the measurements with no object in the beam and the division means that corresponding members of the vectors are divided. Idealizing the transformation $\mathbf{L}(\mathbf{A})$ as linear, the logarithm of the measurements with noise is

$$\mathbf{L}_{with\_noise} = \mathbf{M_{ave}A} + \mathbf{w} \quad (15)$$

where, for this model, $\mathbf{M_{ave}} = {}^{\partial L}/_{\partial \mathbf{A}}$ is assumed to be constant and the noise $\mathbf{w}$ probability distribution is a multivariate normal with zero mean and constant covariance. With this model, the linearized maximum likelihood estimator is [15]

$$\hat{\mathbf{A}}_{MLE} = \left[\left(\mathbf{M_{ave}}^T \mathbf{C}_L^{-1} \mathbf{M_{ave}}\right)^{-1} \mathbf{M_{ave}^T C_L^{-1}}\right] \mathbf{L_{with\ noise}} \quad (16)$$

where $\mathbf{C_L}$ is the assumed constant covariance of the noise. The factor in brackets of (16) can be pre-computed as a single matrix, so the linear MLE is a matrix multiplication times the measurement vector $\mathbf{L_{with\ noise}}$. The form of this estimator is unchanged for higher dimensions although, of course, the matrix dimensions will change.

It should be emphasized that the A-table estimator operates over the full range of the object and the data to test it are computed using the full nonlinear model in equations (2). In the linear model, the $\mathbf{M_{ave}}$ matrix is the slope of the transformation $\mathbf{L}(\mathbf{A})$ at an operating point. Since the transformation is close to linear, $\mathbf{M_{ave}}$ is approximately constant throughout the range of input data.

The other parameter of the estimator, the noise covariance $\mathbf{C_L}$, varies inversely with the number of photons so it depends exponentially on $\mathbf{A}$ and is obviously not constant. However, examining the linear estimator in (16), we note that if k is a constant, multiplying the covariance by k results in an inverse $(k\mathbf{C_L})^{-1} = {}^1/_k \mathbf{C_L^{-1}}$. If we replace $\mathbf{C_L}$ by $k\mathbf{C_L}$ in the estimator, the first factor in the bracket of (16), $\left(\mathbf{M^T C_L^{-1} M}\right)^{-1}$, is proportional to k and the second factor, $\mathbf{M^T C_L^{-1}}$, is proportional to ${}^1/_k$. The two constant factors cancel out and the linear MLE is unchanged if the covariance is multiplied by a constant. Since the covariance depends on the number of photons in each PHA bin and all the measurements are multiplied by the object transmission, changing $\mathbf{A}$ does not affect the estimator to a first approximation. Due to the larger attenuation coefficients at low energy, as $\mathbf{A}$ increases the low energy measurements are attenuated more than the high energy measurements so the effect of changing $\mathbf{A}$ is not simply to multiply the covariance by a constant but the relative sizes of the elements of $\mathbf{C_L}$ are changed. The empirical Monte Carlo results show that the change is small enough so that the noise covariance of the A-table estimator is close to the CRLB throughout the range of $\mathbf{A}$ tested. This is the justification for the use of the linearized estimator.

The method to compute the $\mathbf{M_{ave}}$ and $\mathbf{C_L}$ matrices from calibration data is described in Sec. II-F.

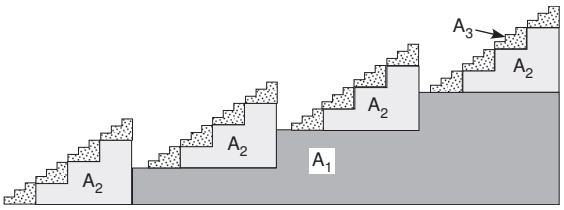

Fig. 2. Three material calibration phantom. Step wedges of three materials with known thicknesses provide known A-vectors at points in the three dimensional space. The transmitted flux through the calibration phantom is measured using the clinical x-ray system. The measurements are done with high counts so they have low noise. The measurement data are stored by the system computer in a memory to be used during data acquisition to compute the correction vector. See the estimator block diagram in Fig. 1.

E. A Calibration phantom for the estimator parameters

The purpose of the calibration phantom is to provide low noise values of the measurement vector $\mathbf{L}$ for a set of points in three dimensional A-space. A side-view of a three material phantom is shown in Fig. 2. If we use the attenuation coefficient functions of the materials of the calibrator as the basis set[16], then the $\mathbf{A}$ vectors for each step are simply the thicknesses of the materials along lines from the x-ray source to the detector. The phantom can be constructed from stable, machinable materials such as acrylic plastic and aluminum. The third material could be, as an example, a plastic resin with molecular linked iodine whose attenuation simulates iodine contrast agent in blood[17].

The calibrator data are acquired with the clinical x-ray imaging system without requiring additional physics instruments. A long exposure time or an average of multiple exposures is used to produce low noise data. To measure all parts of the phantom, it can be moved through the x-ray system with a mechanical stage or a CT scanner patient positioning table. With a fan beam system, the actual path lengths through different parts of phantom can be computed from its dimensions, the known geometry of the x-ray system by developing a method to locate the calibrator accurately with respect the the scanner gantry such as affixing pins to the phantom and scanning it. Fig. 2 shows a phantom with uniform steps but exponentially spaced thicknesses provide better results since they have closer spaced samples in the region near the origin where the gradient of $\mathbf{L}$ is highest. Points that are not on an evenly spaced lattice in A-space can be accommodated by the error-correcting method described in Sec. II-G.

F. Linear MLE parameters from calibration data

As discussed previously, we need $\mathbf{M_{ave}}$ and $\mathbf{C_L}$ to implement the linear estimator in (16). The matrix $\mathbf{M_{ave}}$ is the gradient of $\mathbf{L}(\mathbf{A})$ so we can approximate it as the coefficients of a least squares fit of all the calibrator measurements $\mathbf{L}_{calibrator}$ as a function of the calibrator A-vector values. This gives an average value over the range of $\mathbf{A}_{calibrator}$. The covariance $\mathbf{C_L}$ is estimated from the sample covariance of the measurements in a region of the phantom with constant $\mathbf{A}$ vector close to the center of the A-vector region spanned by the calibrator. See the discussion in Sec. II-D on the effect of the variation of $\mathbf{C_L}$ with $\mathbf{A}$ on the linear MLE.

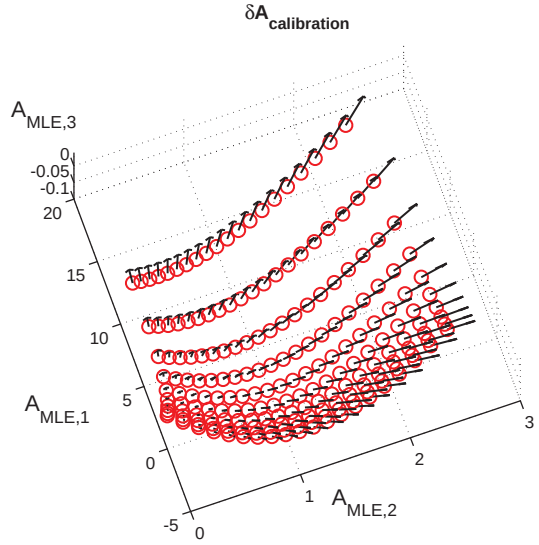

Fig. 3. Correction vectors for the initial linear MLE from calibration data. The circles are the linear MLE estimates and the the lines are the correction vectors from the estimates to the actual A-vector values. Note that the corrections are three dimensional vectors. Only a sample of the points is shown and the correction vectors are scaled for clarity. The units of the axes are g/cm^2.

G. Delaunay triangulation for interpolating corrections in higher dimensions

Computing the corrections to the initial linear maximum likelihood estimates requires interpolation of unequally spaced data in higher dimensions. The interpolation method used in the previous implementation[5] was based on an algorithm[18] that fits a semi-flexible two dimensional plate to the estimates. This algorithm is not readily extended to higher dimensions so a new approach is required.

Fig. 3 illustrates the computation of the correction vectors. If we apply the linear estimator to the calibration data, we get the correction values, which are a set of irregularly spaced points in 3D space shown as the circles in Fig. 3. The corrections are the vectors from the linear MLE values to the known A-vectors for each step of the calibrator. These correction vectors are shown as arrows in the figure.

To compute the correction for a measurement during the scan, we need to interpolate in the table of correction vectors using the linear MLE value for the measurement. Since these points are unequally spaced, we cannot use ordinary interpolation algorithms designed for equally spaced tables. For the estimator of this paper, linear interpolation on a Delaunay triangulation[19] of the calibration points is used.

The Delaunay triangulation is the subdivision of the points into simplexes that maximizes the minimum angle of all the simplex's angles. A simplex is a higher dimensional extension of a two dimensional triangle. In three dimensions, it is a tetrahedron. The triangulation is pre-computed so the processing of a measurement involves locating the enclosing simplex and computing the interpolated correction vector $\delta\mathbf{A}$ as a linear combination of the correction vectors at the vertices of the enclosing simplex multiplied by the barycentric coordinates.

In the Monte Carlo simulation, the interpolation is computed using the Matlab $scatteredInterpolant$ function. Open source code to compute the Delaunay triangulation ($delaunayn$) and the enclosing simplex and the barycentric coordinates ($tsearchn$) is provided by the Octave project[20].

The Delaunay triangulation method is applicable with two, three or higher dimensions. Notice that the interpolation dimension is equal to the A-vector dimension. This can be much smaller than the measurements dimension, which is the number of PHA bins of the photon counting detector.

H. Points outside the calibration convex hull

Due to noise, the initial linear estimate, $\hat{\mathbf{A}}_{MLE}$, may be outside the convex hull of the calibration data (see Fig. 4). For these points we can use linear extrapolation of the data on the nearest calibration data points. This extrapolation method was sufficient to provide good performance in the simulations but clearly other methods, such as inverse distance weighted extrapolation, can be used. Most of the out of range points occurred for small object thicknesses, which have low noise, so the deviations from the calibration convex hull are small. For small thicknesses, the initial estimates may have negative values and it is not possible for calibration data to span these values. The calibrator dimensions were adjusted so points in the objects with large A-vector values were within the calibrator convex hull.

I. Optimal PHA energy bins

The PHA bins used in the simulation were computed with an algorithm that maximized the SNR with the CRLB as the covariance

$$SNR^2 = (\delta\mathbf{A})^T \mathbf{C}^{-\mathbf{1}}_{\mathbf{A},\mathbf{CRLB}} (\delta\mathbf{A})$$

The algorithm used as a signal $\delta\mathbf{A} = [0,\ 0,\ -1]^T$. That is, the imaging task was to detect changes in the third A-vector components with other components fixed. The results however were not sensitive to this choice and were the same if, for example, $[-1,\ 0,\ 0]^T$ or $[0,\ -1,\ 0]^T$ were used. The SNR was optimized by exhaustively searching all possible bin widths summing to the maximum energy in the spectrum with an increment of 3 keV. The transmitted spectrum with an A-vector in the center of the calibrator was used.

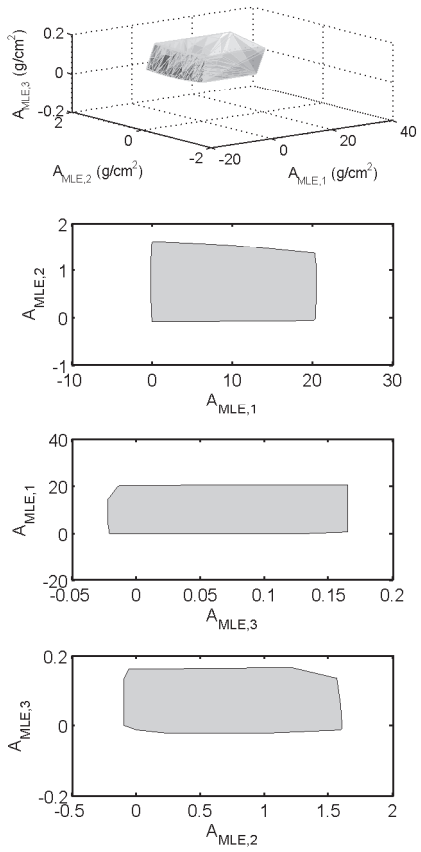

Fig. 4. The convex hull of the linear maximum likelihood estimates of the calibration data. The calibrator shown in Fig. 2 has step wedge thicknesses that are in a rectangular region of A-vector space. Because of the nonlinearity of $\mathbf{L}(\mathbf{A})$, the linear estimator outputs are in the non-rectangular space shown. The initial estimates $\hat{\mathbf{A}}_{MLE}$ may fall outside the convex hull because of noise so the interpolator needs to be able to extrapolate outside this hull. The top plot is a three dimensional representation. The bottom three plots are the projections of the convex hull onto the three coordinate planes. The units of the axes are g/cm^2.

J. Iterative estimator with Monte Carlo data

An iterative estimator was implemented and tested with Monte Carlo data. The estimator assumes that the spectra $S_k(E)$ and the attenuation coefficients of the basis materials[16] are known. It computes the logarithm of the likelihood of the PHA counts in (5) for a specified A-vector using equations (2) to compute the λ_k and with the photon counts $n_k,\ k = 1 \ldots nspect$ for each measurement. The A-vector that maximizes the log-likelihood is computed using the Matlab function $fminsearch$, which implements the Nelder-Mead simplex direct search algorithm. Open source code for this function is provided by Octave[20].

K. Monte Carlo simulation

The performance of the estimators was studied using a Monte Carlo simulation. The simulation compared the mean squared error of the estimates to the Cramèr-Rao lower bound.

A 120 kilovolt x-ray tube spectrum was generated using the TASMIP algorithm of Boone and Seibert[21]. The number of photons incident on the object, which is the integral of the spectrum, was assumed to be 10^6. As discussed in Sec. II-E, a basis set consisting of the attenuation coefficients of acrylic plastic, aluminum, and an iodine contrast agent simulant consisting of 20% fraction by weight iodine in paraffin ($C_{31}H_{64}$ molecular composition) was used. The attenuation coefficients were computed by piece-wise continuous Hermite polynomial interpolation of the standard Hubbell-Seltzer tables[22].

The random data for each A-vector were generated by computing the transmitted flux through the object with the TASMIP x-ray tube spectrum and the basis material attenuation coefficients. The transmitted photons were incident on a photon counting detector with five bin PHA. The detector was assumed to be perfectly absorbing so the energy of each photon was measured with no added noise. The expected value of the counts in each bin was computed from the transmitted spectrum using (2). The PHA energy bins were determined as described in Sec. II-I. The PHA response functions were assumed to be perfect rectangles and the detector was assumed to have negligible pulse pileup so the counts in each bin were independent Poisson random variables. Random Poisson distributed PHA counts with these expected values were generated.

A calibration phantom with 30 steps for each material was implemented. The thicknesses were geometrically spaced from zero to 20, 1.5 and 0.125 g/cm^2 for each of the calibration materials respectively. These were chosen to be greater than the object values so all estimates except for noise will fall within the estimates' data convex hull. The phantom transmission data for all steps and the sample covariance at one step in the calibration phantom were computed by averaging 300 sets of random data. These were used as the parameters of the A-table estimator. In a CT scanner, each set would correspond to a single angle projection so the tube loading to acquire the calibration data is equivalent to approximately a single scan.

Objects with A-vectors on three lines through the A-vector space (see panel (a) of Fig. 5) were used. Each line is the A-vectors of different thicknesses of a material whose attenuation coefficient can be approximated by different ratios of the basis materials' attenuation coefficients[23]. The end points of the lines in A-vector space and therefore the ratios were $[16,\ 1.2,\ 0.1]$, $[5,\ 0.9,\ 0.1125]$, and $[16,\ 0.375,\ 0.1]\ g/cm^2$.

The same random counts were used by each of the estimators to compute the estimates of the A-vectors. Since the input data are random, the estimates are also random quantities so multiple trials were used. The mean square error MSE of the estimates for these trials was computed as

$$\mathbf{MSE} = \frac{1}{N_{trials}} \sum_{i=1}^{N_{trials}} \left(\hat{\mathbf{A}} - \mathbf{A_{actual}}\right)^2 \qquad (17)$$

where $\hat{A}$ was the estimate, $\mathbf{A_{actual}}$ was the actual A-vector value, and N_{trials} was the number of random trials, 2000. Notice that the MSE is a vector quantity with a value for each component of $\mathbf{A}$.

The MSE of the A-table and iterative estimators were compared with each other and with the CRLB. The CRLB was calculated as described in Sec. II-C for each point on the lines. The estimates for a specific random sample of the data on Line 1 were also compared directly. The computation times with both estimators were recorded.

III. RESULTS

A. Estimates on three lines in A-space

Fig. 5 shows the Monte Carlo estimates with the A-table estimator for three lines through A-vector space. The estimates are the individual points and the actual values are the solid lines. Panel (a) shows the estimates for data without noise. The other panels are the estimates with noisy data on each of the three lines. The three original lines are included in each panel for reference. Random five bin PHA data were used.

B. MSE vs. CRLB

Fig. 6 shows the Monte Carlo simulation mean squared error for the A-table and iterative estimators as a function of distance from the origin along the three lines shown in Fig. 5. The CRLB is also shown as the solid line. The MSE was computed using (17). Notice that the vertical scale is logarithmic. The A-table estimator results are the diamonds and the iterative estimator are the asterisks. The MSE values are nearly equal so the symbols overlap.

C. Estimates for same random sample

Fig. 7 compares the estimates of the A-table and the iterative estimators for the same random data. The estimates are approximately the same with the differences increasing somewhat for the higher noise data at larger A-vector magnitudes.

D. Optimal PHA energy bins

Fig. 8 shows the optimal PHA energy bins. The bin boundaries are the vertical dashed lines and the arrows show the bins. The attenuation coefficient of iodine and the x-ray tube spectrum are shown for reference.

IV. DISCUSSION

The results in Fig. 6 show that, although there are small random fluctuations, the A-table estimator mean squared errors are essentially equal to the CRLB. As discussed previously, this implies that the bias is negligible compared with the variance and the variance is close to the CRLB. That is, the A-table estimator is efficient. The low bias is also shown by part (a) of Fig. 5 where the estimates with no noise data are close to the actual

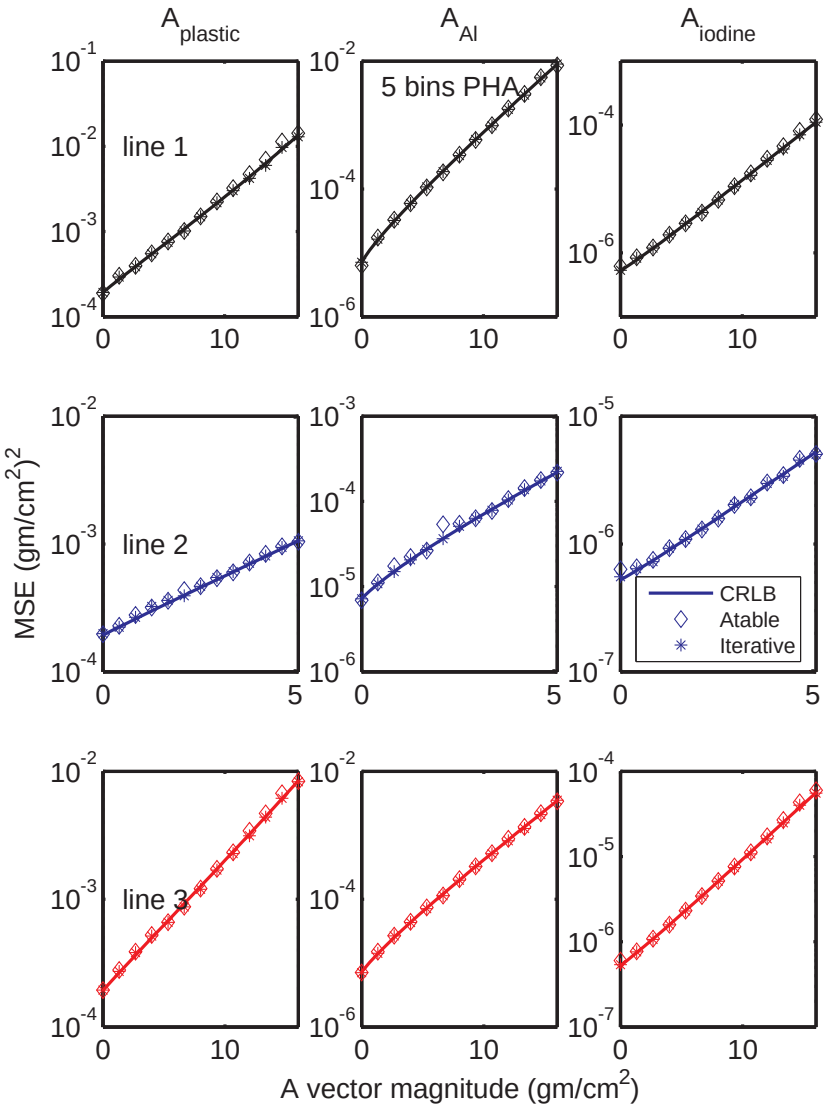

Fig. 6. The mean squared error and the CRLB for the A-table and iterative network estimators as a function of distance from the origin along the three A-space lines in Fig. 5. Five bin PHA data were used. The A-vector components are plotted in columns from left to right and the result for lines (1), (2), and (3) are in rows from top to bottom. The CRLB in each case is shown as a solid line. The A-table estimator is the diamonds and the iterative estimator is the asterisks. Notice that both estimators have MSE close to the CRLB so their symbols overlap.

lines. The averages of A-vector estimates with noisy data shown in the figure are also close to the actual values.

The interpolation errors and therefore the bias depend on the spacing of the calibration points. As more steps are used in the calibration phantom, the interpolation errors decrease but the computation time increases linearly with the number of Delaunay simplexes. A calibrator with 30 steps for each type of material was used in the simulations. If the computation time is a problem it may be possible to pre-compute a finely sampled, regularly spaced, three dimension look up table from the calibration data. The Delaunay interpolator would still be required to compute the regularly spaced table but this would be done before a scan. During data acquisition, the corrections would be computed from the regularly spaced table, which is much faster than interpolation in Delaunay simplexes.

Fig. 6 shows that both the iterative and the A-table estimator have mean squared errors equal to the CRLB. In addition, Fig. 7 shows that the A-table and the iterative estimators produce close to the same estimates with the same random data although there are small differences with the high noise data at large A-vector magnitudes. These two results indicate that the A-table outputs are close to the maximum likelihood estimates and have nearly equivalent statistical properties.

The iterative estimator computation time was approximately 180 times longer than the A-table estimator. The implementations were not optimized for computation speed but this large difference would also be expected for more optimized algorithms.

The optimal PHA energy bins are shown in Fig. 8. Notice that the optimization algorithm, which maximizes SNR for the imaging task described in Sec. II-I, places

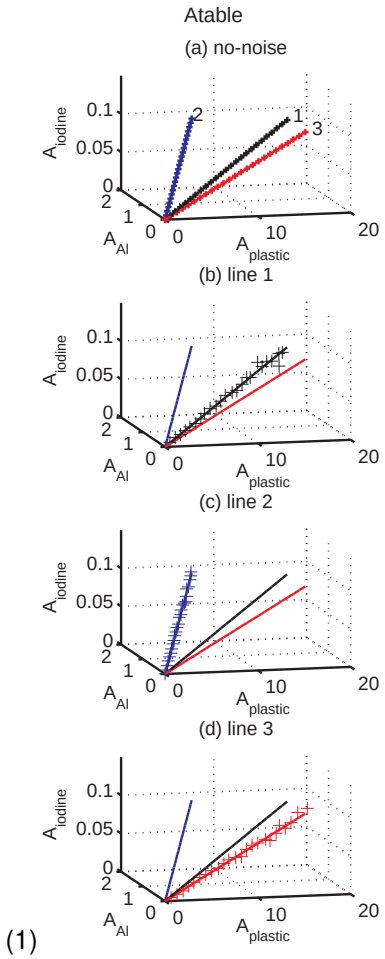

Fig. 5. A-table estimator outputs on three lines in A-space with random five bin PHA data. The estimates are plotted as individual points and the actual lines are solid. Plot (a) shows the estimates from data with no noise. Plots (b) to (c) show the estimates with noisy data for each of the three lines.The original lines are shown for reference.

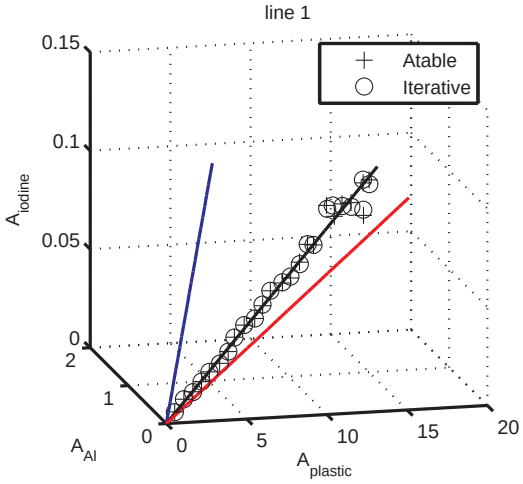

Fig. 7. Estimates with A-table and iterative estimator for same random sample of data. The data are for one trial with the points on line 1.

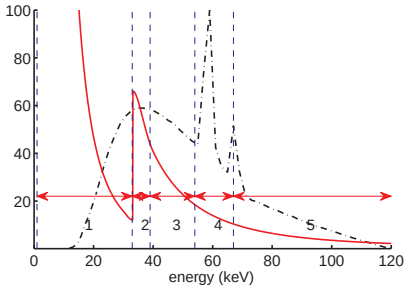

Fig. 8. Optimal PHA bins. The PHA bin edges are shown as the vertical dashed lines; the bins are the horizontal arrows. The attenuation coefficient of iodine (solid line) and the x-ray tube spectrum (dashed line) are also shown for reference. Notice that there is a bin edge at the k-edge of iodine, 33.2 keV. The optimal bins are computed as described in Sec. II-I.

a bin boundary at the K absorption edge of the iodine contrast material. The photons with energies smaller than the K-edge have high information content so the algorithm allocates a bin for these energies even though they are highly attenuated by the object.

Current state-of-the-art photon counting detectors for medical imaging have artifacts such as pulse pileup, charge sharing, K-fluorescence radiation escape, and others[24], [2]. Although the detector technology is advancing rapidly, estimators will need to utilize data with some levels of these artifacts and methods to correct the errors and to utilize data with errors are an important area of research. Since the A-table estimator calibrator data have errors similar to those in patient scans, the correction step in the estimator implementation will also correct some of the errors. However, the correction is not complete and additional methods to utilize data with experimental errors are a subject of current research.

Utilization of the three dimensional A-vector data to produce clinically useful information is an important problem that is the subject of current research. Images of the third component, or its reconstruction in CT, provide indicators of the distribution of contrast material within the patient with minimal contributions from the surrounding body structures. These could be superimposed on lower noise images of the anatomy created from the other components as described in a previous paper[23]. Methods similar to those previously used with two dimension data[25] could exploit the correlation of the noise in the individual A-vector components to produce lower noise images with material selective information.

V. CONCLUSION

A non-iterative estimator for use with a three function basis set approximation to the attenuation coefficient is described. The three function approximation can be used to represent the attenuation coefficients of a high atomic number contrast agent and body materials. The estimator can be used with data from photon counting detectors with multi-bin PHA. The parameters required to implement the estimator can be derived from measurements

of a calibration phantom with the clinical x-ray system and do not require measurements of the source spectrum or the detector energy response functions. The performance of the estimator was evaluated using a Monte Carlo simulation and it was found to achieve the CRLB over a wide range of operating conditions. Therefore, we are guaranteed that no other unbiased estimator can have a smaller variance. The estimator outputs with the same random data are close to the output of an iterative maximum likelihood estimator.

REFERENCES

[1] M. Aslund, E. Fredenberg, M. Telman, and M. Danielsson, "Detectors for the future of X-ray imaging," *Radiat. Prot. Dosim.*, vol. 139, pp. 327–333, 2010.

[2] K. Taguchi and J. S. Iwanczyk, "Vision 20/20: Single photon counting x-ray detectors in medical imaging," *Med. Phys.*, vol. 40, p. 100901, 2013.

[3] R. E. Alvarez and A. Macovski, "Energy-selective reconstructions in X-ray computerized tomography," *Phys. Med. Biol.*, vol. 21, pp. 733–44, 1976.

[4] R. E. Alvarez, "Dimensionality and noise in energy selective x-ray imaging," *Med. Phys.*, vol. 40, no. 11, p. 111909, 2013.

[5] ——, "Estimator for photon counting energy selective x-ray imaging with multi-bin pulse height analysis," *Med. Phys.*, vol. 38, pp. 2324–2334, 2011. [Online]. Available: http://www.ncbi.nlm.nih.gov/pubmed/21776766

[6] K. C. Zimmerman, E. Y. Sidky, and T. Gilat Schmidt, "Experimental study of two material decomposition methods using multi-bin photon counting detectors," *Proc. SPIE*, vol. 9033, pp. 90 333G–6, 2014. [Online]. Available: http://dx.doi.org/10.1117/12.2043679

[7] P. L. Rajbhandary, S. S. Hsieh, and N. J. Pelc, "Segmented targeted least squares estimator for material decomposition in multi bin pcxds," *Proc. SPIE*, vol. 9033, pp. 903 319–903 319–9, 2014. [Online]. Available: http://dx.doi.org/10.1117/12.2043198

[8] S. M. Kay, *Fundamentals of Statistical Signal Processing, Volume I: Estimation Theory* . Upper Saddle River, NJ: Prentice Hall PTR, 1993, vol. Sec. 4.5.

[9] ——, *Fundamentals of Statistical Signal Processing, Volume I: Estimation Theory* . Upper Saddle River, NJ: Prentice Hall PTR, 1993, vol. Ch. 3.

[10] ——, *Fundamentals of Statistical Signal Processing, Volume I: Estimation Theory* . Upper Saddle River, NJ: Prentice Hall PTR, 1993.

[11] E. Roessl and R. Proksa, "K-edge imaging in x-ray computed tomography using multi-bin photon counting detectors," *Phys. Med. Biol.*, vol. 52, pp. 4679–4696, 2007.

[12] J. P. Schlomka, E. Roessl, R. Dorscheid, S. Dill, G. Martens, T. Istel, C. Bäumer, C. Herrmann, R. Steadman, G. Zeitler, A. Livne, and R. Proksa, "Experimental feasibility of multi-energy photon-counting K-edge imaging in pre-clinical computed tomography," *Phys. Med. Biol.*, vol. 53, pp. 4031–4047, 2008.

[13] S. M. Kay, *Fundamentals of Statistical Signal Processing, Volume I: Estimation Theory* . Upper Saddle River, NJ: Prentice Hall PTR, 1993, vol. Ch. 7.

[14] "DESY PHOTON SCIENCE." [Online]. Available: http://photon-science.desy.de/

[15] S. M. Kay, *Fundamentals of Statistical Signal Processing, Volume I: Estimation Theory* . Upper Saddle River, NJ: Prentice Hall PTR, 1993, vol. Ch. 4.

[16] R. E. Alvarez and E. J. Seppi, "A comparison of noise and dose in conventional and energy selective computed tomography," *IEEE Trans. Nucl. Sci.*, vol. NS-26, pp. 2853–2856, 1979.

[17] QRM-Gmbh, "QRM-CTiodine." [Online]. Available: http://www.qrm.de/content/pdf/QRM-CTiodine.pdf

[18] J. D'errico, "Surface Fitting using gridfit." [Online]. Available: MATLABCentralFileExchange,http://www.mathworks.com/matlabcentral/fileexchange/8998),

[19] M. de Berg, M. van Kreveld, M. Overmars, and O. Schwarzkopf, *Computational Geometry: Algorithms and Applications*. Berlin Heidelberg: Springer, 2013.

[20] "GNU Octave." [Online]. Available: https://www.gnu.org/software/octave/

[21] J. M. Boone and J. A. Seibert, "An accurate method for computer-generating tungsten anode x-ray spectra from 30 to 140 kV," *Med. Phys.*, vol. 24, pp. 1661–70, 1997.

[22] J. H. Hubbell, "Review of photon interaction cross section data in the medical and biological context," *Phys. Med. Biol.*, vol. 44, pp. R1–R22, 1999.

[23] R. E. Alvarez, "Near optimal energy selective x-ray imaging system performance with simple detectors," *Med. Phys.*, vol. 37, pp. 822–841, 2010.

[24] M. Overdick, C. Baumer, K. J. Engel, J. Fink, C. Herrmann, H. Kruger, M. Simon, R. Steadman, and G. Zeitler, "Towards direct conversion detectors for medical imaging with X-rays," *IEEE Trans. Nucl. Sci.*, vol. NSS08, pp. 1527–1535, 2008.

[25] Q. Cao, T. Brosnan, A. Macovski, and D. Nishimura, "Least squares approach in measurement-dependent filtering for selective medical images," *IEEE Trans. Med. Imag.*, vol. 7, pp. 154–160, 1988.